(31) E. J. Laskowski and D. N. Hendrickson, *Inorg. Chem.*, **17**, 457 (1978).
(32) K. S. Murray, *Coord. Chem. Rev.*, **12**, 1 (1974).
(33) H. J. Schugar, G. R. Rossman, and H. B. Gray, *J. Am. Chem. Soc.*, **91**, 4564 (1969).
(34) T. C. Gibb, R. Greatrex, and N. N. Greenwood, *J. Chem. Soc. A*, 890 (1968).
(35) V. I. Goldanski, G. M. Gorodinskii, S. V. Karyagin, L. A. Korytko, L. M. Krizhanskii, E. F. Makarov, I. P. Suzdalev, and V. V. Khrapov, *Dokl. Akad. Nauk SSSR*, **147**, 127 (1962).
(36) S. V. Karyagin, *Dokl. Akad. Nauk SSSR*, **148**, 1102 (1963).
(37) M. Blume, *Phys. Rev. Lett.*, **14**, 96 (1965).
(38) M. Gerloch, J. Lewis, F. E. Mabbs, and A. Richards, *J. Chem. Soc. A*, 112 (1968).
(39) A. N. Buckley, G. V. H. Wilson, and K. S. Murray, *Solid State Commun.*, **7**, 471 (1969).
(40) J. Lewis, F. E. Mabbs, and A. Richards, *J. Chem. Soc. A*, 1014 (1967).
(41) M. Cox, B. W. Fitzsimmons, A. W. Smith, L. F. Larkworthy, and K. A. Rogers, *Chem. Commun.*, 183 (1969).
(42) A. N. Buckley, I. R. Herbert, B. D. Rumbold, G. V. H. Wilson, and K. S. Murray, *J. Phys. Chem. Solids*, **31**, 1423 (1970).

Contribution from the School of Chemical Sciences, University of Illinois, Urbana, Illinois 61801

Magnetic Exchange Interactions in Binuclear Transition-Metal Complexes. 17. Benzidine and *p*-Phenylenediamine, Extended Aromatic Diamine Bridging Ligands in Binuclear Copper(II) 2,2′,2″-Triaminotriethylamine and Vanadyl Bis(hexafluoroacetylacetonate) Complexes[1]

TIMOTHY R. FELTHOUSE and DAVID N. HENDRICKSON*[2]

Received February 13, 1978

The preparation and magnetic properties are reported for a series of ten binuclear copper(II) complexes of the form $[Cu_2(tren)_2(DA)](Y)_4$, where tren is 2,2′,2″-triaminotriethylamine, DA represents an aromatic diamine such as *p*-phenylenediamine (PPD), durenediamine (DDA), benzidine (BZD), *o*-tolidine (OT), or 4,4′-methylenedianiline (MDA) and Y^- is variously NO_3^-, ClO_4^-, or PF_6^-. Additionally, three vanadyl complexes of the form $[VO(hfac)_2]_2(DA)$ have been prepared, where $hfac^-$ is 1,1,1,5,5,5-hexafluoroacetylacetonate and DA is PPD, DDA, or BZD. The copper(II) binuclear complexes are the first discrete compounds to be isolated containing redox-active aromatic diamines. Variable-temperature (4.2–286 K) magnetic susceptibility and EPR data are reported for all complexes. Antiferromagnetic exchange interactions are found for all copper(II) complexes with exchange parameters which range from ca. -3 cm^{-1} for the BZD-bridged complexes to nearly -35 cm^{-1} for the PPD-bridged complexes. No interactions could be detected in the vanadyl complexes with PPD and DDA, but $[VO(hfac)_2]_2(BZD)$ was found to contain only one unpaired electron per binuclear complex. A molecular orbital analysis of the aromatic diamines reveals a tendency to favor a predominantly σ superexchange pathway between the two distorted trigonal-bipyramidal copper(II) centers, although a distinct separation of σ and π orbitals can not be found. These results in conjunction with the recently determined structure of $[Cu_2(tren)_2(BZD)](NO_3)_4$ demonstrate that electrons can exchange between two copper(II) ions separated by more than 12 Å via the BZD bridging group. The interrelationships between the interactions involved in binuclear exchange-interacting metal complexes and inner-sphere electron transfer between two metal complexes are presented.

Introduction

The previous papers[1,3-16,18] in this series have sought to establish various criteria for judging the viability of a particular single-atom or polyatomic bridging unit to support a magnetic exchange interaction between two paramagnetic metal ions. Much of this work has been concerned with exchange interactions in binuclear or dimeric copper(II) complexes and has indicated that the strength of the exchange interaction depends primarily upon the symmetry and energy of the copper(II) ion ground state relative to the highest occupied molecular orbitals of the bridging moiety. For example, in binuclear copper(II) complexes bridged by oxalate,[12] squarate,[12] and the dianions of 2,5-dihydroxybenzoquinones,[13] as shown below, the largest exchange interaction is found for the

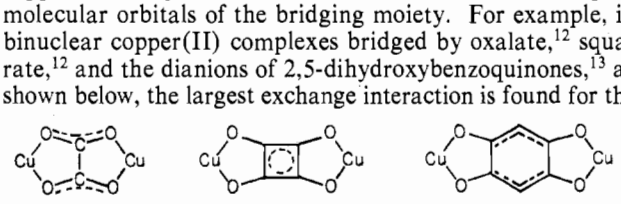

μ-oxalate complex as expected on the basis of the Cu–Cu separation, but the next largest interaction is found for the dihydroxybenzoquinone complex and not the squarate complex. Apparently, the greater number of proper symmetry orbitals and their energy proximity to the copper(II) orbitals in the dihydroxybenzoquinone dianion accounts for the greater interaction as compared to the squarate orbitals. The same trend is observed for nickel(II) complexes bridged by these dianions.

Recently, our work[11-14,17,18] has emphasized the importance of the transition-metal ground state in propagating an exchange interaction across a polyatomic bridging unit. In particular, trigonal-bipyramidal complexes of copper(II) with 2,2′,2″-triaminotriethylamine (tren) have been found to be quite effective in obtaining an exchange interaction across an extended bridging moiety. Initially, "outer-sphere" dimers of the form $[Cu_2(tren)_2(X)_2](BPh_4)_2$, where X^- is Br^-,[9] Cl^-,[9] OH^-,[9] CN^-,[19] NCO^-,[5] and NCS^-,[5] were prepared and found to show antiferromagnetic interactions with J (in the Hamiltonian $-2J\hat{S}_1\cdot\hat{S}_2$) ranging from -3.5 to -0.05 cm^{-1}. The X-ray crystal structures[9,19] of four of these dimers revealed a novel Cu–X···H–N–Cu hydrogen-bonded pathway for the exchange interactions. Inner-sphere bridged complexes involving the $Cu(tren)^{2+}$ unit have led to larger antiferromagnetic exchange interactions. For example, cyanide[11] and imidazolate[18] bridges have shown exchange interactions of -88 and -38 cm^{-1}, respectively. In an effort to extend the length of the bridging unit and still maintain an exchange interaction between the copper(II) ions, we chose to investigate various aromatic diamines.

Although heterocyclic diamines (i.e., pyrazine and related bifunctional bridges) have been used extensively to study electron dynamical phenomena such as exchange interactions,[20-22] mixed-valence systems,[23-25] and redox reactions,[24,26,27] aromatic diamines as potential mediators of electron exchange

0020-1669/78/1317-2636$01.00/0

largely have been unexplored. In this paper we examine $Cu(tren)^{2+}$ complexes bridged by the following aromatic diamines:

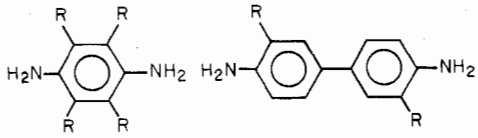

PPD, R = H
DDA, R = CH_3

BZD, R = H
OT, R = CH_3

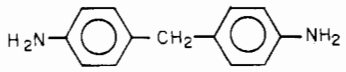

MDA

The complexes are of the form $[Cu_2(tren)_2(DA)](Y)_4$, where DA represents an aromatic diamine including *p*-phenylenediamine (PPD), durenediamine (DDA), benzidine (BZD), *o*-tolidine (OT), or 4,4′-methylenedianiline (MDA) and Y^- is variously NO_3^-, ClO_4^-, or PF_6^-. Variable-temperature magnetic susceptibility (4.2–286 K) and EPR data are reported on these compounds and interpreted in light of our recent X-ray structure determination of $[Cu_2(tren)_2(BZD)](NO_3)_4$. A preliminary account of some of these results has appeared.[28] Finally, the magnetic properties are reported for three binuclear vanadyl complexes of the form $[VO(hfac)_2]_2(DA)$ where $hfac^-$ is 1,1,1,5,5,5-hexafluoroacetylacetonate and DA is PPD, DDA, or BZD. These complexes provide an opportunity to observe the effect of altering the metal ion (Cu^{2+} to VO^{2+}) and its ground state (d_{z^2} to d_{xy}) on the magnetic exchange interaction.

Experimental Section

Compound Preparation. The nonbridging ligands 2,2′,2″-triaminotriethylamine (Ames Laboratories, Inc.) and 1,1,1,5,5,5-hexafluoroacetylacetone (Columbia Organic Chemicals) were used as received. The aromatic diamines were purchased from commercial sources as follows: benzidine (Sigma), *o*-tolidine (Eastman), 4,4′-methylenedianiline (Aldrich), *p*-phenylenediamine (Eastman), and 2,3,5,6-tetramethyl-*p*-phenylenediamine (Aldrich). All diamines were used as received except *p*-phenylenediamine which was recrystallized from benzene and further purified by vacuum sublimation at least once at ca. 140 °C. Additional chemicals were at least reagent grade. Elemental analyses were performed by the microanalytical laboratory of the School of Chemical Sciences, University of Illinois. The analytical data for all compounds are compiled in Table I.[29]

$[Cu_2(tren)_2(BZD)](NO_3)_4$ was prepared by mixing a filtered 50-mL 95% ethanol solution of $Cu(NO_3)_2 \cdot 3H_2O$ (1.20 g, 5 mmol) and tren (0.75 g, 5 mmol) with 30 mL of a 95% ethanol solution containing BZD (0.46 g, 2.5 mmol). A dark green microcrystalline solid formed immediately and was collected and washed with a little ethanol and then ether. Crystals may be grown by slow diffusion of the two 95% ethanol solutions described above or by slow evaporation of a 95% ethanol solution of the solid.

$[Cu_2(tren)_2(BZD)](ClO_4)_4$ was prepared by combining a 50-mL aqueous solution of $Cu(ClO_4)_2 \cdot 6H_2O$ (1.85 g, 5 mmol) and tren (0.75 g, 5 mmol) with 50 mL of a 95% ethanol solution of BZD (0.46 g, 2.5 mmol) and evaporating to ca. 80 mL. A lime green solid formed and was collected, washed with ether, and dried under vacuum over P_4O_{10}. Dark green crystals may be grown from acetonitrile but are "bow-tie" shaped.

$[Cu_2(tren)_2(BZD)](PF_6)_4$ was prepared from an 80-mL aqueous solution of $CuSO_4 \cdot 5H_2O$ (1.25 g, 5 mmol), tren (0.75 g, 5 mmol), and BZD (0.46 g, 2.5 mmol). The undissolved BZD was gradually solubilized by the addition of 40 mL of 95% ethanol. An excess of NH_4PF_6 (3.0 g, 18.4 mmol) was dissolved in a minimum of 95% ethanol and added to the mixture. After evaporating for ca. 3 h in a hood, a microcrystalline green product was collected, washed with water and then ether, and dried under vacuum over P_4O_{10}.

$[Cu_2(tren)_2(OT)](PF_6)_4$ was prepared by combining $CuSO_4 \cdot 5H_2O$ (1.25 g, 5 mmol) and tren (0.75 g, 5 mmol) with a twofold excess of OT (1.1 g, 5.2 mmol) in a 100-mL 1:1 water–95% ethanol mixture. Another 100 mL of 95% ethanol was added to help dissolve the OT which dissolved upon heating. An excess of NH_4PF_6 (3.0 g, 18.4 mmol) in 30 mL of water was added to the hot solution. Evaporation overnight to ca. 80 mL produced a brown solid which was washed with ether and then redissolved in 400 mL of methanol. The recrystallized product formed shiny brown sheets upon evaporation which crushed to a lime green powder.

$[Cu_2(tren)_2(MDA)](NO_3)_4$ was prepared by adding a 50-mL methanol solution of MDA (0.5 g, 2.5 mmol) to a 50-mL methanol solution of $Cu(NO_3)_2 \cdot 3H_2O$ (1.20 g, 5 mmol) and tren (0.75 g, 5 mmol). The resulting mixture was filtered and a green microcrystalline solid formed upon standing. The solid was collected, washed with ether, and dried over P_4O_{10} in a vacuum desiccator.

$[Cu_2(tren)_2(MDA)](ClO_4)_4$ was prepared by mixing $Cu(ClO_4)_2 \cdot 6H_2O$ (1.85 g, 5 mmol) dissolved in 30 mL of 95% ethanol, tren (0.75 g, 5 mmol), and then a 50-mL 95% ethanol solution of MDA (0.5 g, 2.5 mmol). The resulting blue-green solution was filtered and an excess of $NaClO_4$ (3.0 g, 24.5 mmol) dissolved in 95% ethanol was added to induce precipitation. A microcrystalline bright green solid soon formed and was collected, washed with ether, and dried in a vacuum desiccator over P_4O_{10}.

$[Cu_2(tren)_2(PPD)](NO_3)_4$ was prepared by mixing a filtered 30-mL methanol solution of $Cu(NO_3)_2 \cdot 3H_2O$ (1.20 g, 5 mmol) and tren (0.75 g, 5 mmol) with a 25-mL methanol solution containing PPD (0.26 g, 2.5 mmol). A dark green solid formed immediately and was washed with ether and dried in a vacuum desiccator over P_4O_{10}.

$[Cu_2(tren)_2(PPD)](ClO_4)_4$ was prepared by adding an excess of $NaClO_4$ (5.0 g, 41.0 mmol) dissolved in 20 mL of water to 80 mL of a filtered aqueous solution containing $CuSO_4 \cdot 5H_2O$ (1.25 g, 2.5 mmol). The dark green microcrystalline product which forms immediately should be collected rapidly to avoid further reaction of PPD[30] which leads to the eventual formation of a dark brown solid. The green product was washed with water and ether and then dried in a vacuum desiccator over P_4O_{10}. Green crystals of the complex formed from a 150-mL aqueous mixture of $Cu(ClO_4)_2 \cdot 6H_2O$ (1.85 g, 5 mmol), tren (0.75 g, 5 mmol), and PPD (0.26 g, 2.5 mmol), but much of the brown solid also was suspended in the mixture. These were suitable for X-ray diffraction (vide infra).

$[Cu_2(tren)_2(PPD)](PF_6)_4$ was prepared as per the ClO_4^- salt except NH_4PF_6 (3.0 g, 18.4 mmol) was substituted for $NaClO_4$. The green solid formed after ca. 30 min in the aqueous mixture and should be filtered off promptly to avoid further reaction of PPD.[30] The solid was washed with water and ether and dried in a vacuum desiccator over P_4O_{10}.

$[Cu_2(tren)_2(DDA)](PF_6)_4$ was prepared as the PPD salt except the DDA (0.45 g, 2.5 mmol) was solubilized using 95% ethanol. The microcrystalline green product was washed with water and then ether and dried in a vacuum desiccator over P_4O_{10}.

Samples of **$VO(hfac)_2 \cdot H_2O$** were prepared using a procedure suggested for $VO(tfac)_2$[31] [tfac = 1,1,1-trifluoro-2,4-pentanedione]. In a typical preparation $VOSO_4 \cdot 2H_2O$ (4.75 g, 2.39 mmol) was dissolved in 200 mL of water acidified with ca. 0.5 mL of concentrated sulfuric acid to prevent hydrolysis. Slightly more than a twofold excess of 1,1,1,5,5,5-hexafluoroacetylacetone (10.00 g, 4.81 mmol) was added to the solution followed by enough 95% ethanol to dissolve any precipitate. The solution was filtered and neutralized to a pH of 5.5 (pH meter) with dilute aqueous sodium carbonate. The end point showed a dark green coloration in the solution. The solution was extracted with three 200-mL portions of benzene. The extracted solution was dried with $MgSO_4$, filtered, and evaporated to give ca. 4.0 g of crude **$VO(hfac)_2 \cdot H_2O$**. This product proved satisfactory for use in further preparations.

Samples of **$[VO(hfac)_2]_2(PPD)$** and **$[VO(hfac)_2]_2(DDA)$** were prepared in similar fashion. To a filtered 60-mL dichloromethane solution of $VO(hfac)_2 \cdot H_2O$ (0.76 g, 1.52 mmol) was added PPD (0.05 g, 0.46 mmol) or DDA (0.08 g, 0.49 mmol) in 25 mL of dichloromethane. The addition of the PPD solution caused the greenish brown solution of $VO(hfac)_2 \cdot H_2O$ to turn purple. The solution was concentrated to 40 mL by gentle heating whereupon a pinkish brown microcrystalline product formed. The product was collected, washed with dichloromethane, and dried under vacuum over P_4O_{10}. The yield was 0.33 g (66.7%); mp 148 °C. When the DDA solution was added, little color change in the green solution was observed when concentrated to 40 mL. A light green product was collected and dried under vacuum over P_4O_{10}. The yield was 0.35 g (63.8%); mp 110 °C.

$[VO(hfac)_2]_2(BZD)$ was prepared by mixing a filtered 60-mL dichloromethane solution of $VO(hfac)_2 \cdot H_2O$ with a 20-mL di-

chloromethane solution of BZD (0.09 g, 0.49 mmol). The mixture was heated to boiling and concentrated to 30 mL. After 30 min of heating, a microcrystalline pinkish purple product formed from the intensely purple solution. Two crops were collected and combined which upon drying under vacuum over P_4O_{10} gave 0.37 g (66.1%); mp 145 °C.

Physical Measurements. Variable-temperature (4.2–286 K) magnetic susceptibility data were obtained using a Princeton Applied Research Model 150A vibrating-sample magnetometer operating at 12.7 kG and calibrated with $CuSO_4 \cdot 5H_2O$ as described in a previous paper.[3] All data were corrected for diamagnetism[32] and TIP (taken as 60×10^{-6} cgsu/mol of Cu(II)). All least-squares fittings were performed using a new version of the minimization computer program STEPT.[33]

EPR spectra of powdered samples were recorded on a Varian E-9 X-band spectrometer and a Varian E-15 Q-band spectrometer as described previously.[12]

Molecular Orbital Calculations. The MO calculations were performed using the CNDO/2 method.[34] The molecular geometries of BZD and PPD were idealized on the basis of average bond distances and angles obtained in the X-ray diffraction study of $[Cu_2(tren)_2(BZD)](NO_3)_4$.[28] The C–H, N–H, and C–N bond lengths were taken as 1.05, 1.05, and 1.45 Å, respectively. The C–C single bond between the phenyl rings in BZD was taken as 1.50 Å and all C–C distances in the phenyl rings were assigned values of 1.38 Å. Angles about all C atoms were taken as 120° while angles about the N atoms were assumed to be 109.5°.

Results

Variable-temperature (4.2–286 K) magnetic susceptibility data were collected for solid samples of all ten binuclear copper(II) complexes bridged by BZD, OT, MDA, PPD, or DDA. For complexes with BZD, PPD, and DDA as bridging ligands, an antiferromagnetic exchange interaction was observed with a maximum in the magnetic susceptibility data. The BZD- and OT-bridged complexes as PF_6^- salts exhibited weak antiferromagnetic exchange interactions with no peak in the magnetic susceptibility. The magnetic susceptibilities of the MDA-bridged complexes showed essentially Curie-law behavior.

The data for the BZD- and OT-bridged complexes were first fit to the Bleaney–Bowers equation[35] as shown in eq 1. In

$$\chi_M = \frac{Ng^2\beta^2}{kT}\left[\frac{2}{3 + \exp(-2J/kT)}\right] + N\alpha \qquad (1)$$

eq 1, N, β, k, T, and J have their usual meaning and the temperature-independent paramagnetism, $N\alpha$, was assigned as previously indicated. Because the exchange interactions in these complexes were small, i.e., magnetic susceptibility maxima occurred below 10 K, it was felt that the data could be better fit to an expression which includes the effects of Zeeman splitting of the triplet-state energy levels. Hence, when $2J \simeq g\beta H$, then for H = 12.7 kG and $g \simeq 2.1$, the magnetic Zeeman interaction approaches the magnitude of the singlet–triplet separation ($2J$), i.e., $g\beta H = 1.2$ cm^{-1}. The magnetic susceptibility expression was derived using a spin Hamiltonian of the form

$$\hat{H} = -2J\hat{S}_1 \cdot \hat{S}_2 + g_\parallel \beta \hat{H} \cdot \hat{S} + \tfrac{1}{2} g_\perp \beta \hat{H}(\hat{S}_+ + \hat{S}_-) \qquad (2)$$

where the first term accounts for the isotropic exchange interaction and the last two terms describe the electronic Zeeman interaction. In eq 2, J is the exchange parameter, $\hat{S}_1$ and $\hat{S}_2$ are the spin operators for metal centers 1 and 2, $g_\parallel$ and $g_\perp$ are the electronic g values for the complex, β is the Bohr magneton, $\hat{H}$ is the magnetic field, $\hat{S}$ is the spin operator projected onto the quantization axis, and $\hat{S}_+$ and $\hat{S}_-$ are the raising and lowering spin operators. The magnetic susceptibility for these binuclear complexes was obtained with a Hamiltonian matrix diagonalization procedure as detailed in the Appendix. The results, however, with this treatment were essentially identical with those using eq 1 and, therefore, only the results obtained from eq 1 are reported in Tables II–V[29] for the four complexes bridged by BZD or OT.

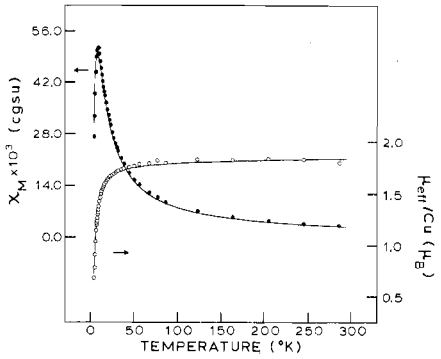

Figure 1. Experimental molar paramagnetic susceptibility (●) per binuclear complex and effective magnetic moment (○) per Cu(II) ion vs. temperature for $[Cu_2(tren)_2(BZD)](NO_3)_4$. The solid lines represent the least-squares fit using the Bleaney–Bowers equation.

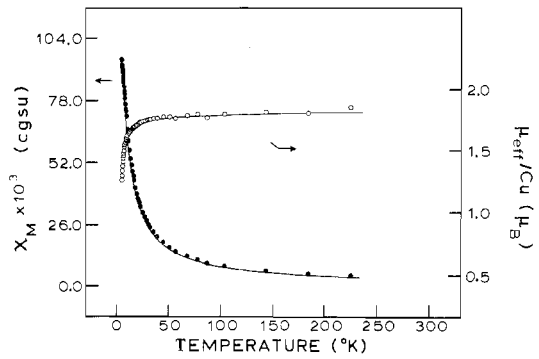

Figure 2. Experimental molar paramagnetic susceptibility (●) per binuclear complex and effective magnetic moment (○) per Cu(II) ion vs. temperature for $[Cu_2(tren)_2(OT)](PF_6)_4$. The solid lines were generated from the least-squares fit using the Bleaney–Bowers equation.

A plotting of the magnetic susceptibility and effective magnetic moment vs. temperature is illustrated in Figure 1 for one preparation of the crystallographically characterized complex $[Cu_2(tren)_2(BZD)](NO_3)_4$. The experimental magnetic susceptibility increases as the temperature is lowered until a maximum is reached at 8.3 K, after which there is a rapid decrease in χ_M down to 4.2 K. The μ_{eff}/Cu values over the temperature range vary from 1.78 μ_B at 286 K to 0.67 μ_B at 4.2 K. Least-squares fitting of the data using eq 1 gives $J = -4.5$ cm^{-1} and $g = 2.09$. A second preparation of this complex produced essentially identical results ($J = -4.5$ cm^{-1} and $g = 2.13$). The solid lines in Figure 1 illustrate the fit obtained using eq 1.

The magnetic susceptibility data for the ClO_4^- and PF_6^- salts of the binuclear cation $[Cu_2(tren)_2(BZD)]^{4+}$ showed similar results. The data for $[Cu_2(tren)_2(BZD)](ClO_4)_4$ exhibited a maximum in the magnetic susceptibility at 7.0 K. The μ_{eff}/Cu value ranged from 1.90 μ_B at 224 K to 0.88 μ_B at 4.2 K. Least-squares fitting of these data to eq 1 gave $J = -3.7$ cm^{-1} and $g = 2.13$. The PF_6^- salt showed a slightly weaker interaction with no susceptibility maximum and least-squares fitting parameters (eq 1) of $J = -3.3$ cm^{-1} and $g = 2.15$.

Compared with the binuclear copper(II) complexes bridged by BZD, a weaker interaction was found for $[Cu_2(tren)_2(OT)](PF_6)_4$. The μ_{eff}/Cu value decreases from 1.85 μ_B at 224 K to 1.26 μ_B at 4.2 K. The least-squares fit data are shown in Figure 2 with the solid lines representing the theoretical least-squares-fit curve from eq 1. The curve is generated with the parameters $J = -2.4$ cm^{-1} and $g = 2.08$ and a truly ex-

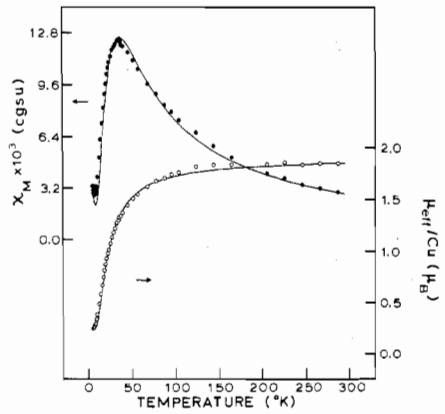

Figure 3. Experimental molar paramagnetic susceptibility (●) per binuclear complex and effective magnetic moment (○) per Cu(II) ion vs. temperature for $[Cu_2(tren)_2(PPD)](PF_6)_4$. The solid lines represent the least-squares fit to the Bleaney–Bowers equation with the inclusion of a paramagnetic impurity (eq 3).

cellent fit of the data occurs below 38 K such that the experimental points in Figure 2 mask most of the theoretical solid line.

The two complexes with MDA as the bridging ligand have magnetic susceptibility data which follow the Curie law; i.e., the μ_{eff}/Cu value remains essentially constant throughout the temperature range from 286 to 4.2 K. The μ_{eff}/Cu value averages to 1.83 μ_B for $[Cu_2(tren)_2(MDA)](NO_3)_4$ while the value for the ClO_4^- salt averages to 1.82 μ_B. The magnetic susceptibility data are tabulated for both compounds in Table VI.[29]

The four complexes bridged by PPD or DDA all showed magnetic susceptibility maxima greater than 25 K and minima below 10 K followed by an increase in the susceptibility. The latter behavior is characteristic of a small amount of paramagnetic impurity in the sample. In order to account for this behavior a $S = {}^1/_2$ impurity term was added to eq 1 giving the modified equation (3). In eq 3, the parameter p gauges

$$\chi_M = (1-p)\left(\frac{Ng^2\beta^2}{kT}\right)\left[\frac{2}{3+\exp(-2J/kT)}\right] + N\alpha + p\left(\frac{Ng^2\beta^2}{4kT}\right) \quad (3)$$

the amount of paramagnetic impurity that is present in the sample (% impurity = 100p). The least-squares-fit data are compiled in Tables VII–X.[29] The average g value for the monomeric impurity was assumed to be the value found for the binuclear complex from the ca. 300 K Q-band EPR spectrum (vide infra).

The strongest antiferromagnetic exchange interaction of all of the compounds in this study was found for $[Cu_2(tren)_2(PPD)](NO_3)_4$. A maximum in the magnetic susceptibility data occurs near 67.0 K. The μ_{eff}/Cu value ranges from 1.80 μ_B at 286 K to 0.34 μ_B at 4.2 K. The least-squares fit parameters from eq 3 are $J = -35.1$ cm^{-1}, $g = 2.21$, and $p = 0.0690$.

The ClO_4^- and PF_6^- salts of the $[Cu_2(tren)_2(PPD)]^{4+}$ cation show somewhat weaker antiferromagnetic exchange interactions with magnetic susceptibility maxima at 41.1 and 32.2 K, respectively. Least-squares fitting of the data for $[Cu_2(tren)_2(PPD)](ClO_4)_4$ to eq 3 gives $J = -26.2$ cm^{-1}, $g = 2.17$, and $p = 0.0435$. A plotting of the experimental data for $[Cu_2(tren)_2(PPD)](PF_6)_4$ is given in Figure 3. The μ_{eff}/Cu value ranges from 1.83 μ_B at 286 K down to 0.23 μ_B at 4.2 K. The solid lines represent the least-squares fit to eq 3 with $J = -19.8$ cm^{-1}, $g = 2.17$, and $p = 0.0321$.

Table XII. Summary of Magnetic Susceptibility and EPR Parameters for Aromatic Diamine-Bridged Copper(II) and Vanadyl Binuclear Complexes

compound	J, cm^{-1}	$\bar{g}$[a]	g_1[b]	g_2	g_3
$[Cu_2(tren)_2(BZD)](NO_3)_4$	−4.5	2.09	2.031	2.127	2.190
$[Cu_2(tren)_2(BZD)](ClO_4)_4$	−3.7	2.13	2.016	2.132	2.197
$[Cu_2(tren)_2(BZD)](PF_6)_4$	−3.3	2.15	2.015	2.154	2.178
$[Cu_2(tren)_2(OT)](PF_6)_4$	−2.4	2.08	2.013	2.141	2.198
$[Cu_2(tren)_2(MDA)](NO_3)_4$	$\lesssim$0.5[c]	2.108	2.035[d]	2.123	2.158
$[Cu_2(tren)_2(MDA)](ClO_4)_4$	$\lesssim$0.5[c]	2.117	2.026	2.153	2.173
$[Cu_2(tren)_2(PPD)](NO_3)_4$	−35.1	2.21	2.011	2.142	2.192
$[Cu_2(tren)_2(PPD)](ClO_4)_4$	−26.2	2.17	2.057	2.118	2.158
$[Cu_2(tren)_2(PPD)](PF_6)_4$	−19.8	2.17	2.062	2.092	2.197
$[Cu_2(tren)_2(DDA)](PF_6)_4$	−17.6	2.21	2.012	2.133	2.206
$[VO(hfac)_2]_2(PPD)$	$\lesssim$0.5[c]	1.978	1.978[e]		
$[VO(hfac)_2]_2(DDA)$	$\lesssim$0.5[c]	1.979	1.979[e]		

[a] Average g values obtained from the magnetic susceptibility fitting except if $|J| \lesssim 0.5$ cm^{-1}; then EPR values are given. [b] These g values were obtained from the 300 ca. K Q-band EPR spectra of powdered samples. [c] In these cases there are the signs of an exchange interaction in the magnetic susceptibility down to 4.2 K and, as such, $|J| \lesssim 0.5$ cm^{-1}. [d] Another derivative was found at $g = 2.053$. [e] In these cases only a single derivative was obtained.

Substitution of DDA for PPD as a bridging ligand produced the compound $[Cu_2(tren)_2(DDA)](PF_6)_4$ which showed a somewhat weaker interaction than was seen for the PPD-bridged complexes. A maximum in the magnetic susceptibility was found at 26.6 K. The μ_{eff}/Cu value ranges from 1.83 μ_B at 224 K to 0.52 μ_B at 4.2 K. This relatively high μ_{eff} value at 4.2 K indicates the presence of a paramagnetic impurity which is clearly reflected by the fact that the magnetic susceptibility passes through a minimum at 9.1 K and *then increases*. Least-squares fitting of the susceptibility data gives $J = -17.6$ cm^{-1}, $g = 2.21$, and $p = 0.1583$.

Three complexes of the form $[VO(hfac)_2]_2(DA)$ were prepared, where DA is PPD, DDA, and BZD. The variable-temperature magnetic susceptibility data have been collected and the experimental results are summarized in Table XI.[29] In each case the susceptibility data closely follow Curie-law behavior, i.e., the μ_{eff} value remains relatively constant. For the PPD- and DDA-bridged binuclear complexes the μ_{eff}/V value *averages* to 1.70 and 1.63 μ_B, respectively, over the entire temperature range. An unexpected result was obtained for $[VO(hfac)_2]_2(BZD)$. The μ_{eff}/V value begins at 1.30 μ_B at 286 K and gradually drops to 1.20 μ_B at 4.2 K. The *average* μ_{eff}/V value over that temperature range was found to be 1.23 μ_B. The result was reproduced with a second collection of data. The value of 1.23 μ_B per binuclear cluster nearly corresponds to the spin-only value for *one* unpaired electron per cluster, i.e., $[n(n+2)]^{1/2}/m^{1/2} = 3^{1/2}/2^{1/2} = 1.22$ μ_B, where n is the number of unpaired electrons and m is the number of paramagnetic metal ions in the cluster. A summary of the least-squares-fit exchange parameters and the g values determined from the ca. 300 K Q-band EPR spectra for all compounds studied is presented in Table XII.

EPR spectra were recorded at both X- and Q-band frequencies for the binuclear copper(II) and vanadyl complexes. The spectra were taken at ca. 300 K and near liquid-nitrogen temperatures (ca. 80–110 K) for both frequencies. The copper(II) complexes showed no additional features (Cu hyperfine, zero-field splittings, or half-field $\Delta M_s = 2$ transitions) in the EPR spectra from one temperature to the other. Cooling the samples to ca. 110 K in the Q-band EPR spectrum produced some narrowing of the line widths but no significant changes in the overall spectra. Only the ca. 300 K spectra are reported in the figures.

Figure 4 demonstrates the effect upon the Q-band spectrum of varying the counterion while retaining the same $[Cu_2$-

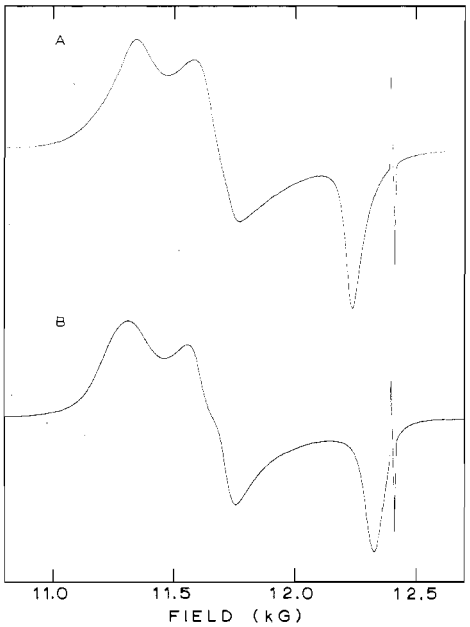

Figure 4. Q-Band (~35 GHz) EPR spectra of powdered samples of $[Cu_2(tren)_2(BZD)](NO_3)_4$ (A) and $[Cu_2(tren)_2(BZD)](ClO_4)_4$ (B) recorded at ~300 K. The DPPH ($g = 2.0036$) resonances were used to calibrate the frequency.

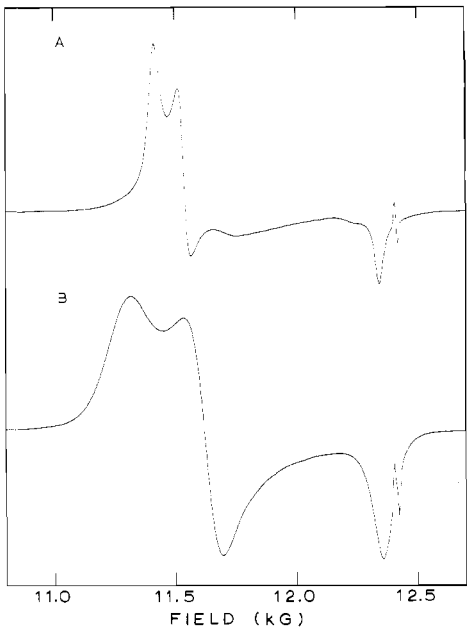

Figure 5. Q-Band (~35 GHz) EPR spectra of powdered samples of $[Cu_2(tren)_2(BZD)](PF_6)_4$ (A) and $[Cu_2(tren)_2(OT)](PF_6)_4$ (B) at ~300 K with DPPH as a frequency calibrant.

$(tren)_2(BZD)]^{4+}$ binuclear cation composition. Tracing A illustrates the 300 K Q-band EPR spectrum for the structurally characterized complex $[Cu_2(tren)_2(BZD)](NO_3)_4$. The rhombic spectrum has g values at 2.190, 2.127, and 2.031. The ClO_4^- analogue in tracing B shows approximately the same g values in the $g_\perp$ region (2.197, 2.132), but a $g_\parallel$ value (2.016) closer to the expected[36] free-electron value of 2.0023 for an unpaired electron in a predominantly d_{z^2} orbital.

The Q-band EPR spectrum of $[Cu_2(tren)_2(BZD)](PF_6)_4$ in Figure 5, tracing A, displays yet another pattern for the $[Cu_2(tren)_2(BZD)]^{4+}$ cation with relatively narrow line widths and a more compact $g_\perp$ region (2.178, 2.154). The $g_\parallel$ value of 2.015 again is close to the expected free-electron value. In contrast, the OT-bridged complex $[Cu_2(tren)_2(OT)](PF_6)_4$,

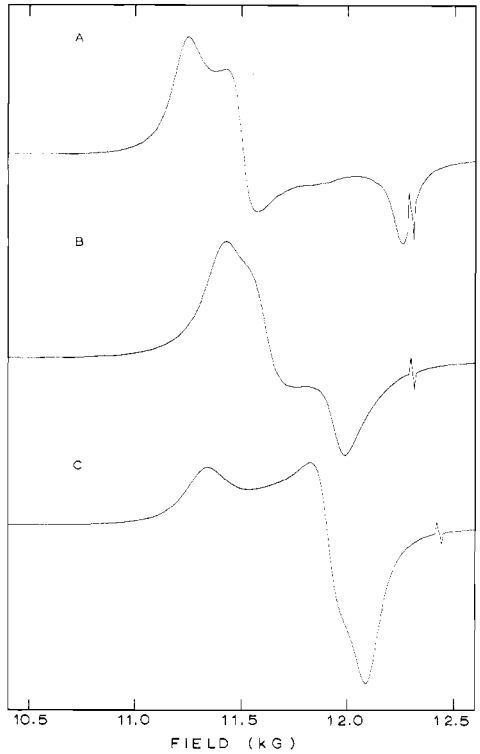

Figure 6. Effect of different counterions on the Q-band (~35 GHz) EPR spectra of powdered samples of $[Cu_2(tren)_2(PPD)](Y)_4$ at ~300 K, where $Y^- = NO_3^-$ (A), ClO_4^- (B), and PF_6^- (C). The DPPH signals are used for calibration of the frequency.

which differs from the BZD complex by only two 3,3′-substituted methyl groups, shows in tracing B much broader spectral features with g values at 2.198, 2.141, and 2.013.

An even greater variation in the 300 K Q-band EPR spectra was observed for the complexes involving the $[Cu_2(tren)_2(PPD)]^{4+}$ cation and these spectra are presented in Figure 6. In tracing A, the $[Cu_2(tren)_2(PPD)](NO_3)_4$ complex shows a rhombic EPR signal with the $g_\perp$ region split into two features at 2.192 and 2.142 and a $g_\parallel$ value of 2.011 near the DPPH reference signal of 2.0036. Tracing B shows that there is a shift in the $g_\parallel$ signal to 2.057 as the counterion is changed to ClO_4^-. The $g_\perp$ region displays very little splitting with g values of 2.158 and 2.118. Finally, tracing C for $[Cu_2(tren)_2(PPD)](PF_6)_4$ shows perhaps the greatest deviation from what one would expect for a complex involving a trigonal-bipyramidal $Cu(tren)^{2+}$ moiety. In this tracing the g values of 2.197, 2.092, and 2.062 would tend to indicate a different geometry[11] and a discussion of this spectrum is presented in the next section. The DDA-bridged complex gave an extremely broad Q-band EPR spectrum and its g values are presented in Table XII along with a summary of the EPR g values calculated from the spectra in Figures 4–6.

The Q-band EPR spectra were recorded for undoped powdered samples of all three vanadyl binuclear complexes. The PPD- and DDA-bridged complexes gave unstructured single derivatives with g values of 1.978 and 1.979, respectively. The BZD-bridged complex with only one unpaired electron gave a spectrum with additional features in addition to the main derivative around 1.973 (12 561 G). The low-field portion of the spectrum shows inflections with g values of 2.047, of 2.016, and near 2.0036 (DPPH) with apparent hyperfine features at 2.029 and 2.016. The hyperfine pattern(s) continue on the high-field portion of the spectrum with 11 discernible hyperfine lines observed between 12 721 and 13 351 G. The average spacing between these 11 hyperfine lines is 63 G.

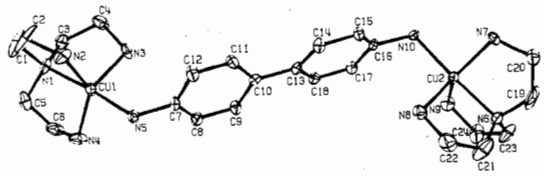

Figure 7. ORTEP plotting of one of the independent binuclear cations in $[Cu_2(tren)_2(BZD)](NO_3)_4$, omitting the hydrogen atoms.

Discussion

Physical Observables. The magnetic susceptibility results summarized in Table XII establish antiferromagnetic exchange interactions for eight of the ten binuclear copper(II) complexes bridged by aromatic diamines. The diamine bridges are varied in extension, i.e., one phenyl vs. two phenyl moieties, and in substituents. The counterions which determine the molecular packing of the binuclear $[Cu_2(tren)_2(DA)]^{4+}$ cations have also been varied. These variations were incorporated to elucidate the factors which influence the magnetic exchange interaction. The tren ligand enforces a basic trigonal-bipyramidal geometry on the copper(II) ion as has been found in all previous structures involving the $Cu(tren)^{2+}$ unit.[9,17,28,37] The tren ligand was selected as the nonbridging ligand, in part, because it prevents the formation of polymeric compounds. More importantly, the tren ligand was selected as the nonbridging ligand because work in these laboratories has shown that the $Cu(tren)^{2+}$ complex is relatively stabilized to reduction. Thus, it has been found that CN^- will not reduce $Cu(tren)^{2+}$ and $\mu(1,2)$-cyano complexes such as $[Cu_2(tren)_2(CN)](PF_6)_3$ have been prepared.[11] It is known that *p*-phenylenediamine is catalytically oxidized by Cu(II) ion centers in several cuproproteins.[38] Likewise, most simple Cu(II) complexes rapidly oxidize *p*-phenylenediamine or benzidine to give upon further reaction dark colored compounds such as Bandrowski's base or benzidine brown. The tren ligand is, then, a very important element needed to isolate these complexes which are the first nonpolymeric Cu(II) complexes of *p*-phenylenediamine and benzidine reported.

As can be seen in Table XII, the exchange parameter does reflect the extension of the bridging diamine. The single phenyl ring in the *p*-phenylenediamine- and durenediamine-bridged complexes leads to an exchange parameter in the range from -17.6 to -35.1 cm^{-1} while the more extended biphenyl moiety in the benzidine- and *o*-tolidine-bridged complexes leads to a weaker antiferromagnetic interaction with J varying from only -2.4 to -4.5 cm^{-1}. The methyl substitution of the phenyl and biphenyl rings potentially can provide both steric and electronic perturbations with resultant changes in the exchange parameter. Finally, a variation in the counterion should affect the relative degree of *inter*molecular interactions throughout the lattice and, hence, allow an assessment of the *intra*molecular nature of the exchange interaction. As a basis for a discussion of the above factors as they affect the observed exchange coupling, the results of the (preliminary, $R = 0.11$) crystal and molecular structure[28] of $[Cu_2(tren)_2(BZD)](NO_3)_4$ will be briefly summarized with emphasis on the structural features that could affect the magnetic properties.

A schematic diagram of the binuclear $[Cu_2(tren)_2(BZD)]^{4+}$ cation is shown in Figure 7. There are two crystallographically different binuclear complexes in the unit cell; however, since both have similar dimensions, only one binuclear unit is illustrated in Figure 7. Each copper(II) ion has a distorted trigonal-bipyramidal coordination geometry with a nitrogen atom of the BZD group bonding into one axial position. The three primary amino groups of the tren ligand occupy the equatorial positions of the trigonal bipyramid with the tertiary tren nitrogen atom positioned in the other axial site. The copper(II) ion is displaced 0.204 Å (average) out of the trigonal plane toward the BZD nitrogen atom. This is typical for $Cu(tren)X^+$ species.[9,17,28,37] The intramolecular Cu–Cu distances are 12.270 (2) and 12.074 (2) Å for the two different binuclear complexes in the compound. Intermolecular Cu–Cu distances as short as 7.499 (2) Å are present. In the solid, the binuclear cations and the nitrate ions are packed together such that weak (>2.9 Å) hydrogen-bonded interactions of the nitrate oxygen atoms and the amino-group nitrogen atoms of the tren and BZD ligands are present. It is important to note that the nitrate oxygen atoms do not bond or even semicoordinate[36] to the copper(II) ions and the shortest oxygen–copper distance is 3.32 (2) Å.

The magnetic properties of $[Cu_2(tren)_2(BZD)](NO_3)_4$ can be interpreted in light of the above structural features. Since there are two different binuclear complexes in the unit cell, it is possible that two exchange parameters would be needed to fit the magnetic susceptibility data displayed in Figure 1. Examination of the experimental data (points) in Figure 1 shows, however, that this is *not* the case. The 8.3 K peak in the magnetic susceptibility vs. temperature curve is not even very broad as would be expected if the two exchange parameters were at all different. Due to the similarity of the copper(II) ion geometries in the two binuclear cations, the key feature distinguishing the two different cations with respect to an exchange pathway appears to be the dihedral angle between the phenyl rings of each BZD bridge. One binuclear cation has a dihedral angle of 13.8° while the other shows a slightly larger angle of 22.5°. In spite of this difference, the susceptibility data do fit to one exchange parameter, $J = -4.5$ cm^{-1}, for this compound.

Before further discussions of the potential of the aromatic diamines to support an exchange interaction can be given, it is necessary to investigate the possibility of alternative exchange pathways, in particular, exchange pathways involving the nitrate or other counterions in the lattice. Nitrate ions have been found[39-41] to support antiferromagnetic exchange interactions, although, in all cases, a direct Cu–O bonding interaction with the nitrate ion is required. For the case of $Cu(NO_3)_2 \cdot 2.5H_2O$, the magnetic susceptibility data have been fit to give $J = -3.6$ cm^{-1} with an isolated-pair model.[39,40] However, the crystallographic results[42] reveal that the pairwise interaction occurs between the hydrogen-bonded chains via a single nitrate oxygen atom. Very recently, the structure[43] and magnetic properties[41] of $Cu(NH_3)_4(NO_3)_2$ have been investigated. This compound exhibits a broad maximum near 5 K in the magnetic susceptibility vs. temperature curve and these results were interpreted as a linear-chain Heisenberg antiferromagnet with $S = {}^1/_2$ and J fit to -2.7 cm^{-1}. The postulated superexchange pathway between two nearby Cu(II) ions does not involve an O–N–O linkage of a nitrate ion but rather occurs between coordinated oxygen atoms of the nitrate ion which stack nearly on top of each other along the c axis. Consequently, in the class of crystallographically characterized copper(II) complexes with nitrate counterions, magnetic susceptibility results reveal relatively weak exchange interactions (-2.7 to -3.6 cm^{-1}) for nitrate ions which are *directly coordinated*, although somewhat weakly (Cu–O distances range from 2.391 (2) to 2.706 (7) Å), and apparently involve only one or two oxygen atoms in the superexchange pathway.

In $[Cu_2(tren)_2(BZD)](NO_3)_4$ no nitrate oxygen atom coordinates to the copper(II) ions. However, the $Cu(tren)^{2+}$ unit has been found to propagate an exchange interaction through a hydrogen-bonded pathway. The greatest interaction of this type has been found[9] for $[Cu_2(tren)_2Br_2](BPh_4)_2$, for which J is -3.5 cm^{-1}. The superexchange pathway involves a Cu–Br···H–N–Cu route. An analogous pathway in $[Cu_2(tren)_2(BZD)](NO_3)_4$ necessarily must involve *two* such hydrogen-bonded pathways. This does not seem to be a viable

route to give an exchange interaction of -4.5 cm^{-1}. Several stronger arguments can be made to support the *intra*molecular nature of the interaction. First, an *inter*molecular exchange pathway would lead to an extended interaction which produces a broadened susceptibility maximum. The susceptibility vs. temperature maximum for $[Cu_2(tren)_2(BZD)](NO_3)_4$ is quite sharp. Secondly, inspection of Table XII shows that as the NO_3^- counterion is replaced by ClO_4^- or PF_6^-, the exchange parameter changes from -4.5 to -3.7 cm^{-1} (ClO_4^-) or -3.0 cm^{-1} (PF_6^-). Such a small variation in J would not be expected if the superexchange pathway involved the counterion. Finally, if the bridge is shortened from benzidine to phenylenediamine, an *increase* in the antiferromagnetic exchange interaction to give an exchange parameter between -19.8 and -35.1 cm^{-1} would surely not be expected if the exchange interaction occurred via a pathway involving the counterion. Therefore, it must be concluded that the principal portion of the observed antiferromagnetic exchange interactions occur via the aromatic diamine bridges in an *intra*molecular fashion.

The Q-band EPR spectra for $[Cu_2(tren)_2(BZD)](Y)_4$, where Y^- is NO_3^-, ClO_4^-, or PF_6^-, and $[Cu_2(tren)_2(OT)](PF_6)_4$, as displayed in Figures 4 and 5, would be expected to give a detailed and sensitive comment on any differences in local copper(II) ion coordination geometry in the series. Unfortunately, the EPR spectra for these compounds will also be responsive to the details of *intra*molecular exchange averaging where, for example, the **g** tensors on the two copper(II) ions are not aligned. *Inter*molecular interactions that are very weak compared to the *intra*molecular interactions can also have quite pronounced effects on the EPR spectra.

The structurally characterized $[Cu_2(tren)_2(BZD)](NO_3)_4$ has four *different* copper(II) sites in the unit cell and tracing A of Figure 4 reflects an "average" of these sites. The rhombic pattern is expected in view of the distorted trigonal-bipyramidal geometry; the $g_\perp$ signal is split into two signals at g values of 2.190 and 2.127, which is caused by the breakdown of the threefold symmetry axis (trigonal plane) of the molecule. The $g_\parallel$ signal at $g = 2.031$ is near the limit reported[36] for copper(II) complexes with trigonal-bipyramidal stereochemistry. In each of the two different binuclear complexes in this compound, the trigonal axes of the two copper(II) ions are not aligned. The trigonal axis (i.e., magnetic z axis) is probably nearly collinear with the Cu–N(BZD) bond vector at each copper(II) ion and in binuclear complex A the angle between the two trigonal axes is ca. 29° (ca. 26° in binuclear complex B). This *intra*molecular misalignment of magnetic axis, in combination with the antiferromagnetic interaction, leads to an averaging of the components of the **g** tensors at the two copper(II) centers. If this is an *inter*molecular interaction that exceeds the copper nuclear hyperfine interaction (ca. 0.02 cm^{-1}), then electrons can also be exchanging between binuclear complexes. An examination of the crystal structure shows that the misalignment between trigonal axes of copper(II) ions in different nearby binuclear complexes can even be greater which could lead to even more dramatic effects on the EPR spectrum. These very weak *inter*molecular interactions would not, of course, necessarily affect the magnetic susceptibility data taken down to 4.2 K. Consequently, the overall EPR resonance pattern could actually reflect a variety of different dynamical processes involving different degrees of magnetic exchange and dipole–dipole interactions both within the binuclear complexes and throughout the solid.

In previous papers[12,14] in this series, the tetraphenylborate anion was found to be effective in magnetically isolating binuclear copper(II) complexes in pure undoped compounds. The large BPh_4^- counterions provided enough shielding between binuclear complexes to give EPR spectra with resolved copper hyperfine and zero-field splittings characteristic of the triplet state of an isolated binuclear copper(II) complex. In the present work, it was, unfortunately, not possible to prepare BPh_4^- salts of either $[Cu_2(tren)_2(BZD)]^{4+}$ or $[Cu_2(tren)_2(PPD)]^{4+}$.

In comparison with the spectrum for the nitrate salt, the Q-band EPR spectrum of $[Cu_2(tren)_2(BZD)](ClO_4)_4$ in Figure 4 (tracing B) shows a shift in the $g_\parallel$ signal to a value of 2.016. Since the $g_\parallel$ signal is nearer to $g_e = 2.0023$ than in the nitrate salt, this could presumably reflect a copper(II) coordination geometry in the perchlorate salt that is closer to an idealized trigonal bipyramid. However, it is possible that this is just a reflection of a difference in weak *inter*molecular interactions. The Q-band spectrum for the PF_6^- salt is shown in Figure 5, tracing A. The narrower line width and decreased splitting in the $g_\perp$ signal ($g = 2.178$ and 2.154) for this compound could again reflect a somewhat different level of *inter*molecular interaction as a consequence of the relatively large PF_6^- counterions. It is also possible that the degree of misalignment of magnetic axes is varying in the series and this leads to the spectral differences. And finally, the spectrum of the *o*-tolidine complex, $[Cu_2(tren)_2(OT)](PF_6)_4$, shown in Figure 5 (tracing B) demonstrates the influence of minor structural changes such as the addition of two methyl groups on the spectral line width.

When the BZD bridge is further extended by incorporating a methylene group between the two phenyl groups to give the MDA bridge, there is no indication of an antiferromagnetic interaction in the magnetism data taken to 4.2 K. This means that $|J| <$ ca. 0.5 cm^{-1} for the two MDA-bridged compounds. Thus, compared to the BZD and OT compounds, the antiferromagnetic interaction is almost an order of magnitude smaller for the MDA compounds. This is most likely due to the saturated methylene group in the bridge. The fact that the MDA compounds do not show an interaction is further substantiation for the suggestion that the anions are not involved in the exchange pathways.

When the extended BZD bridging unit is replaced with the shorter PPD unit, the antiferromagnetic exchange interaction undergoes a six- to eightfold increase. However, considerable variations are found in the magnitude of the exchange parameter for the PPD complexes with a range from -19.8 to -35.1 cm^{-1}. The permethylated PPD bridging unit, DDA, was incorporated in the complex $[Cu_2(tren)_2(DDA)](PF_6)_4$ and a slightly weaker exchange interaction ($J = -17.6$ cm^{-1}) was found as compared to the PPD complex ($J = -19.8$ cm^{-1}). Since this result is contrary to the expected increase in antiferromagnetic interaction resulting from the methyl substituents' donating electron density and leading to an increase in basicity at the nitrogen centers, the observed decrease is apparently due to the steric considerations of the methyl groups affecting the Cu–N(DDA) interaction. Molecular models do indicate the presence of considerable interactions between the DDA methyl groups and the amine groups of the tren ligand.

The Q-band EPR spectra of the NO_3^-, ClO_4^-, and PF_6^- salts of $[Cu_2(tren)_2(PPD)]^{4+}$ are displayed in Figure 6 and present some interesting contrasts in spectral features. Tracing A illustrates the spectrum for the NO_3^- compound which does show the expected rhombic trigonal-bipyramidal pattern ($g = 2.011$, 2.142, 2.192). The g value of 2.011 is the closest to the free-electron value of 2.0023 for any of the compounds in this study. This pattern is clearly indicative of a trigonal-bipyramidal copper(II) coordination geometry with a d_{z^2} ground state. The fact that it is this PPD compound that shows the greatest antiferromagnetic interaction is in keeping with our previous observations of the effectiveness of a predominantly d_{z^2} orbital in transmitting an antiferromagnetic interaction. Tracing B (ClO_4^-) and particularly tracing C (PF_6^-) of Figure 6 are inexplicable in terms of a predominantly d_{z^2} ground state (smallest g values are 2.057 and 2.062, re-

spectively) unless the spectral features can be ascirbed to an exchange-averaging process. Indeed, the PF_6^- compound shows the most unusual pattern where it appears that the $g_\parallel$ signal is at the low-field position. A spectral pattern like this could be taken as indicative of a $d_{x^2-y^2}$ ground state. However, PF_6^- would be expected to have the least tendency to (semi-) coordinate to the copper(II) ion and, as a consequence, it is clear that the copper(II) coordination geometry in $[Cu_2(tren)_2(PPD)](PF_6)_4$ is that of a distorted trigonal bipyramid. An exchange averaging between copper(II) centers with misaligned **g** tensors probably explains this unusual pattern for the PF_6^- compound. The resolution of this problem requires single-crystal X-ray structural work. Along these lines, it is to be noted that, during the preliminary stages of the X-ray diffraction work on $[Cu_2(tren)_2(BZD)](NO_3)_4$, precession and Weissenberg photographs were taken on dark green crystals of $[Cu_2(tren)_2(PPD)](ClO_4)_4$. The possible space groups were found to be $Pca2_1$ [C_{2v}^5; No. 29] with $a = 19.12$, $b = 11.56$, and $c = 16.82$ Å (asymmetric unit includes the binuclear complex) or $Pbcm$ [D_{2h}^{11}; No. 57] with $a = 11.56$, $b = 19.12$, and $c = 16.82$ Å (asymmetric unit includes half of the binuclear complex). The calculated density of 1.65 g/cm^3 agreed fairly well with the observed density of 1.69 g/cm^3 ($CHCl_3/CHBr_3$).

The six-coordinate binuclear vanadyl complexes $[VO(hfac)_2]_2$(PPD) and $[VO(hfac)_2]_2$(DDA) exhibit EPR spectra that are similar to those observed in previous studies.[44,45] For example, a number of adducts of $VO(acac)_2$, where $acac^-$ is acetylacetonate, have been prepared and EPR spectra recorded for benzene solutions.[44] The average g value typically seen for these complexes is 1.9697, which is in reasonable agreement with the values observed for the PPD- and DDA-bridged complexes recorded as powders (see Table XII). Two possible geometries are possible for the PPD and DDA binuclear complexes involving either cis or trans coordination of the aromatic amine group:

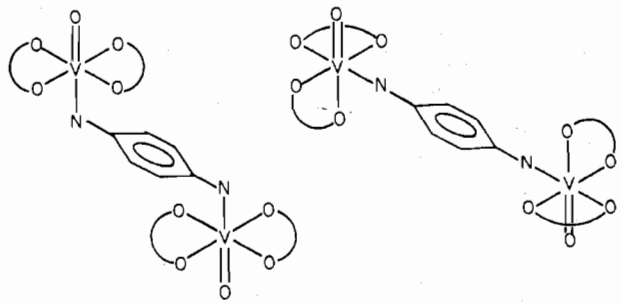

The magnetic susceptibility data for $[VO(hfac)_2]_2$(PPD) and $[VO(hfac)_2]_2$(DDA) do not indicate the presence of any magnetic exchange interaction down to 4.2 K. It is interesting to note that the d_{xy} ground state is ineffective in propagating an exchange interaction through an aromatic ring.

The magnetic susceptibility results for $[VO(hfac)_2]_2$(BZD) indicated that there is one *unpaired electron per binuclear complex*. This was found to be reproducible with a second sample and a redetermination of the susceptibility. Compared to the PPD and DDA compounds, a different formulation is needed for this complex. Benzidine is known[46] to be catalytically oxidized by metal ions and it is possible that the bridging unit is oxidized BZD^+, which has one unpaired electron. Charge balance would require that a hydroxide counterion is present and the compound is $[(VO(hfac)_2)_2(BZD)](OH)$. Analytical data would not easily differentiate between the two compositions. If BZD^+ is bridging between the two $S = {}^1/_2$ VO^{2+} centers, then two of the three previously unpaired electrons could be paired in the complex to leave only one unpaired electron. On the other hand, the compound could be a mixed-valence binuclear vanadium complex with both V(IV) and V(V), which would also leave only one unpaired electron. Mixed-valence V(IV,V) compounds have been reported.[47] The compound is isolated as a microcrystalline pinkish purple compound. In our hands, it has proved impossible to grow crystals large enough to do X-ray diffraction work. Dissolution of the initial microcrystalline solid in various solvents only occurs with a dramatic color change.

Exchange Mechanism. The unpaired electron at each copper(II) center in $[Cu_2(tren)_2(PPD)](Y)_4$ or $[Cu_2(tren)_2(BZD)](Y)_4$ is located in an essentially d_{z^2} orbital. In a binuclear copper(II) complex with each copper(II) center designated A or B, the magnitude of the antiferromagnetic interaction is gauged by the energy separation which develops between the bonding (ϕ_1) and antibonding (ϕ_2) molecular orbitals:

$$\phi_1 \sim d_{z^2}{}^A + d_{z^2}{}^B$$

$$\phi_2 \sim d_{z^2}{}^A - d_{z^2}{}^B$$

The energy separation between ϕ_1 and ϕ_2 develops as a consequence of interactions between the metal d_{z^2} orbitals and the appropriate orbitals of the bridging unit. The energy of the bonding molecular orbital ϕ_1 experiences a greater change in this interaction than does the ϕ_2 orbital and, as a consequence, attention will be focused on the bonding interactions.[48]

Since our crystallographic work[28] has elucidated the structure of the BZD-bridged binuclear complex, the molecular orbital analysis will key on this system. There are two crystallographically different $[Cu_2(tren)_2(BZD)]^{4+}$ species, identified as a binuclear complexes A and B, in the asymmetric unit. The Cu–Cu distances within each of the binuclear cations are 12.270 (2) and 12.074 (2) Å for A and B, respectively. The Cu–N(BZD) distances were found to be normal with a weighted mean of 2.035 ± 0.010 Å. The benzidine amine nitrogen atoms are apparently sp^3 hybridized since the C(BZD)–N(BZD)–Cu angles vary between 111.7 (6) and 116.9 (6)° and are slightly larger than the expected angle of 109.5°. The C–N bond distances of the two different BZD bridges are in the range of 1.417 (13)–1.482 (11) Å. Each of the phenyl rings are planar in the BZD units; however, as was indicated above, the benzidine bridge in either of the two binuclear cations A or B is nonplanar with dihedral angles of 13.8 and 22.5°, respectively, between phenyl rings. The C–C bond distance between the two phenyl rings of the BZD bridge is appropriate for a single bond with an average length of 1.504 ± 0.015 Å.

Relative to the exchange mechanism, the question of greatest interest is whether the intramolecular antiferromagnetic interactions in these complexes are propagated by a predominantly σ- or π-orbital pathway. For the planar biphenyl molecule, which has D_{2h} symmetry, the molecular orbitals are solely of either σ- or π-type character. If a center of inversion is assumed to be present in either the BZD or PPD bridging units, then C_{2h} symmetry is present and this distinguishes to some degree between predominantly σ- or π-orbital exchange pathways. There are no centers of inversion for the binuclear complexes in $[Cu_2(tren)_2(BZD)](NO_3)_4$. The nonzero dihedral angles for the BZD bridges in the two different binuclear complexes in this compound reduce the local symmetry of the bridge to C_1 symmetry. The σ–π separability no longer exists.

Molecular orbital calculations of the CNDO/2 type were performed for various geometries of benzidine and also for *p*-phenylenediamine. The calculations were carried out with the x axis along the N–N vector of the aromatic diamine. For PPD or planar (0° dihedral angle) BZD, the y axis was perpendicular to the plane of the phenyl groups.

In C_{2h} symmetry (center of inversion), the dominantly copper(II) ion molecular orbitals ϕ_1 and ϕ_2 have a_g and b_u

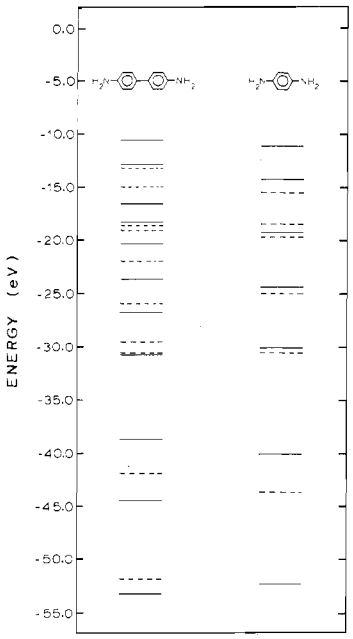

Figure 8. Occupied CNDO/2 molecular orbitals for the BZD (planar configuration) and PPD molecules showing only the a_g (solid lines) and b_u (dashed lines) symmetry orbitals (C_{2h} point group).

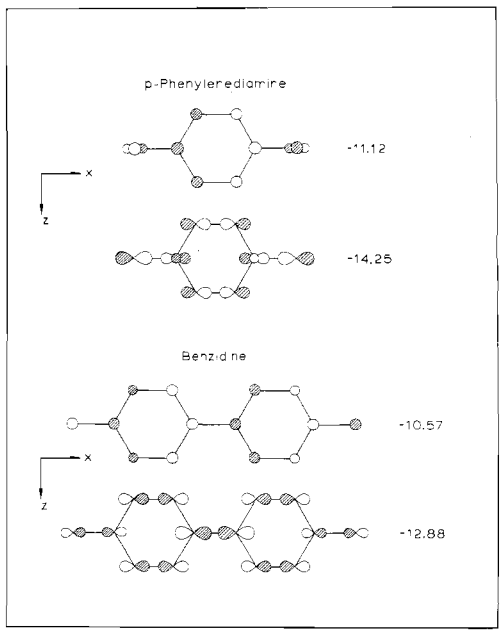

Figure 9. Sketches of the two highest energy occupied a_g-symmetry molecular orbitals for PPD and BZD. The orbital energies are indicated in electron volts. The carbon and nitrogen $2p_x$, $2p_y$, and $2p_z$ contributions to each MO are indicated, where the lobe size of a given atomic orbital is drawn in proportion to the relative contribution of the atomic orbital to that MO. Minor atomic orbital contributions are omitted. In the case of the PPD orbital at −11.12 eV, there is an appreciable nitrogen 2s orbital contribution which was omitted for clarity purposes.

symmetries, respectively. The results of the CNDO/2 calculations for C_{2h}-symmetry PPD and BZD are summarized in Figure 8 in terms of the occupied a_g and b_u BZD or PPD molecular orbitals which can interact with the combination of copper(II) orbitals corresponding to ϕ_1 and ϕ_2. As noted before, the a_g-bonding type of bridge orbital interacts to a greater extent with the copper(II) d_{z^2} orbitals and this results in the majority of the energy difference between the molecular orbitals ϕ_1 and ϕ_2 for the binuclear complex. The a_g-symmetry bridge orbitals that are most effective in providing antiferromagnetic exchange pathways are those that are of higher energy (less negative) because the copper(II) d_{z^2} orbitals are at even higher energy and have good overlap with these bridge orbitals. The a_g-symmetry orbitals of BZD and PPD can be examined with these criteria in mind to identify the most effective bridge orbitals.

Reference to Figure 8 shows that there are some 11 occupied a_g-symmetry molecular orbitals for BZD. The highest energy CNDO/2 orbital of this type is found at −10.57 eV. The composition of this MO is *not* suited for providing an antiferromagnetic interaction between the copper(II) unpaired electrons. The MO is largely of a π type; that is, it is dominantly made up of carbon p_y orbitals and there is essentially a node between the two phenyl rings. Figure 9 gives a sketch of this highest energy a_g-symmetry BZD orbital. The next highest energy a_g-symmetry BZD orbital at −12.88 eV looks promising for an exchange pathway. As illustrated in Figure 9, it can be seen to provide a continuous bonding pathway from one amine nitrogen to the other. It is dominantly comprised of carbon and nitrogen p_x atomic orbitals and, as such, provides a largely σ pathway for an antiferromagnetic exchange interaction. The d_{z^2} ground-state Cu(tren)$^{2+}$ moieties are, after all, best suited for a σ-type exchange interaction. The third and fourth highest a_g-symmetry CNDO/2 orbitals do *not* provide good antiferromagnetic exchange pathways because of nodal properties. Thus, it has to be concluded that of the higher energy a_g-symmetry BZD orbitals the orbital at −12.88 eV is clearly the most effective in providing an antiferromagnetic exchange interaction.

The situation is very similar in the PPD case. Of the three a_g-symmetry orbitals at an energy more positive than −20.0 eV, the second highest orbital at −14.25 eV clearly provides the most effective pathway for an antiferromagnetic interaction. This orbital is sketched in Figure 9 where it can be seen to be largely made up of carbon and nitrogen p_x atomic orbitals. This is another dominantly σ-type pathway.

In comparing the distribution and composition of PPD and BZD molecular orbitals of a_g symmetry, it is possible to understand why the BZD bridge does support an interaction that is not terribly weak relative to the PPD bridge. It would be expected that, compared to the PPD case, the markedly increased extension of the BZD bridge would appreciably attenuate an exchange interaction. This must be offset in part by the availability of more a_g-symmetry orbitals for BZD and also by the fact that the most effective BZD orbital for an exchange pathway is at higher energy that its PPD counterpart.

CNDO/2 calculations were also carried out on BZD molecules where the dihedral angle between the two phenyl rings was taken as either 13.8 or 22.5°, which are the values found for the two different binuclear complexes in $[Cu_2(tren)_2(BZD)](NO_3)_4$. All of the other molecular dimensions were kept fixed. Two observations were made from these calculations. First, the energies of all of the BZD molecular orbitals did not change very much. This is to be expected because the C–C bond distance connecting the two phenyl groups is that of a single C–C bond. For example, the energy for the highest energy a_g (C_{2h} designation) orbital changes from −10.57 to −10.65 eV when the dihedral angle is changed from 0 to 22.5°. Second, the degree of σ–π mixing increases as the dihedral angle in BZD is increased. Thus, the BZD highest energy a_g orbital develops some amount of carbon and nitrogen p_x composition with a nonzero dihedral angle. This would mean that with a nonzero dihedral angle more of the BZD orbitals would become viable antiferromagnetic exchange pathways.

Although the "σ orbitals" of the BZD and PPD bridges effectively propagate the exchange interaction between the copper(II) centers, the involvement of the "π orbitals" cannot

be discounted. In terms of first-order contributions to the superexchange mechanism, the "π orbitals" play an indirect role. When they are of the same symmetry as the largely "σ orbitals", slight admixture of a low-lying π orbitals into σ orbitals that are at higher energy will move the σ orbitals to even higher energy and this can increase the effectiveness of the σ orbital as an exchange pathway. The π orbitals can have a direct effect on the exchange interaction in these $Cu(tren)^{2+}$ complexes, but, of course, this can only occur to second order with configuration interaction of excited states.

The aromatic diamine-bridged binuclear copper(II) complexes in this study have been designed so that the d_{z^2} orbital containing the unpaired electron bonds directly into the diamine nitrogen orbitals. By comparison, previous work[49] has involved the study of magnetic exchange interactions between two copper(II) ions as propagated by 1,2,4,5-tetraiminobenzene and 3,3′,4,4′-tetraiminobiphenyl moieties. The two complexes studied before are

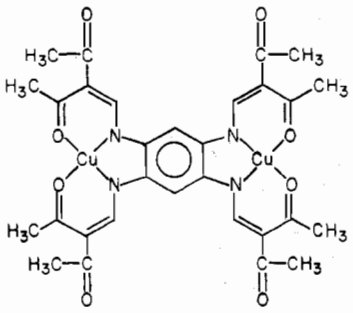

$Cu_2A^4(B^3)_2$

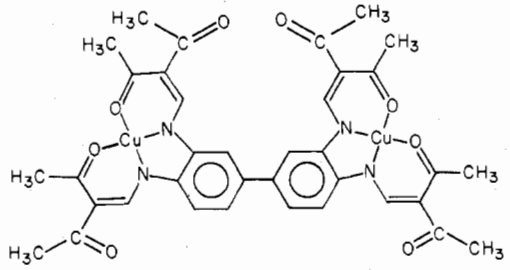

$Cu_2A^3(B^3)_2$

In these two complexes, the copper(II) has a $d_{x^2-y^2}$ ground state. In the case of $Cu_2A^4(B^3)_2$ an antiferromagnetic exchange interaction was found with $J = -12.2$ cm^{-1}. This compares with the smallest J value found in the series $[Cu_2(tren)_2(PPD)](Y)_4$; the PF_6^- salt gives $J = -19.8$ cm^{-1}. The tetraiminobiphenyl unit in $Cu_2A^3(B^3)_2$ was not found to support an exchange interaction; there was no evidence of an interaction in the magnetic susceptibility data taken down to 4.2 K and the EPR spectrum of the binuclear complex doped into the ligand showed copper hyperfine structure characteristic of a monomer, the latter observation indicating that the antiferromagnetic interaction is weaker than the copper hyperfine interaction (≤ 0.02 cm^{-1}).

Magnetic Exchange, Electron Exchange, and Intramolecular Electron Transfer. In this section, the physical basis for a magnetic exchange interaction is briefly reviewed. Also, a qualitative discussion is presented of the interrelationships between the viability of a molecular unit to propagate a magnetic exchange interaction and the rate of *intra*molecular electron transfer across the same molecular unit in a precursor for a redox reaction.

The magnetic exchange interaction in a binuclear complex composed of two paramagnetic transition-metal ions is, of course, not magnetic in origin. It does not result from the through-space interaction of two magnetic dipoles. It has been shown to be electrostatic in nature, as with all chemical bonding phenomena.[50-53] A theoretical evaluation of the exchange parameter for a binuclear copper(II) complex involves setting up the Hamiltonian operator as a sum of kinetic and potential energy terms for all of the electrons in the complex. The potential energy part includes electron–electron repulsion and electron–nucleus attraction terms. Appropriate multielectron determinantal wave functions are then selected, and the Hamiltonian energy matrix is solved for the energies of the various electronic states of the binuclear complex. In the case of an antiferromagnetically coupled copper(II) binuclear complex, the ground electronic state is a singlet ($S' = 0$) with a triplet ($S' = 1$) excited state at an energy of $-2J$. Thus, the exchange parameter J is just a parameter to gauge the energy separation between these two electronic states. The parameter J is a function of Coulomb, exchange, and overlap integrals.

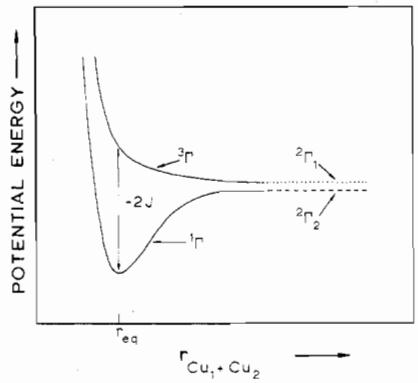

Figure 10. Potential energy diagram for the approach of the two cations $Cu(tren)(BZD)^{2+}$ and $Cu(tren)^{2+}$ oriented in space properly to form $Cu_2(tren)_2(BZD)^{4+}$. The case where there is an antiferromagnetic exchange interaction is illustrated. The interaction between the two doublet-state dications increases with decreasing distance of approach. At the equilibrium Cu_1–Cu_2 distance, r_{eq}, the magnitude of superexchange interaction, is gauged by the exchange parameter J.

The physical meaning of a "magnetic" exchange interaction (or parameter) can be further illustrated by a *gedanken* experiment. Imagine that we know the potential energy curves for the doublet ($S = {}^1/_2$) ground states of trigonal-bipyramidal $[Cu(tren)(BZD)]^{2+}$ and the trigonal moiety $Cu(tren)^{2+}$. If these two cations approach each other in an orientation to form $[Cu_2(tren)_2(BZD)]^{4+}$, two situations could develop. There could be no interaction of the two doublet electronic states as a consequence of the BZD bridge not having orbitals properly constructed to propagate such an interaction. In this case, the exchange parameter J is zero and each doublet state is localized on one copper(II) center.

In the second case, an antiferromagnetic (ferromagnetic) interaction develops as the cations approach each other. Figure 10 illustrates this case. The potential energies of the different states are plotted as a function of the approach coordinate (or distance between copper(II) ions). When the two cations are far apart, each doublet state is localized. As the distance is decreased, the two doublet states interact forming singlet and triplet states for the binuclear complex. The binuclear complex now has a delocalized electronic structure. One important consequence of this delocalized structure is that the unpaired electron and other d electrons associated with one copper(II) ion become involved in an *electron exchange* with the unpaired electron and other d electrons associated with the second copper(II) ion. The effects of so-called Heisenberg spin exchange, in which two free radicals exchange their spins during an encounter, on line widths and saturation charac-

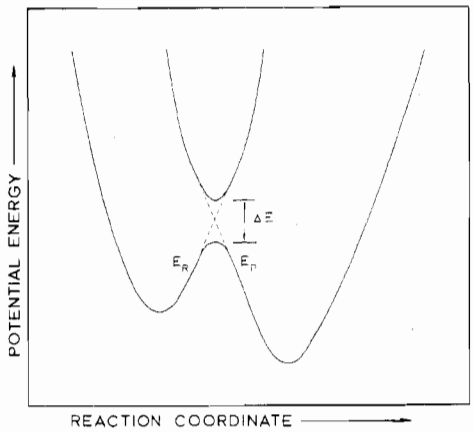

Figure 11. Simplified potential energy diagram for a redox reaction. The parabolic energy curve for the reactants appears to the left of the corresponding curve for the products. The term ΔE is the resonance energy or interaction energy between the two electronic states of the system.

teristics of EPR spectra are well-known.[54-58] For our purposes, however, it is only important that we note that the magnitude of the exchange interaction (J) largely will determine the frequency (ν) of electron exchange so that $\nu \simeq J/h$. Thus, determining the magnitude of the magnetic exchange propagated by some extended bridging group is a means of gauging the viability of that bridging group for supporting electron exchange between the two transition-metal ions.

There has been considerable interest in the study of redox reactions between transition-metal complexes in solution.[59-61] Inner-sphere electron-transfer reactions are of the greatest interest to this paper. Two reactant complexes, A and B, interact to form the precursor (A–B)*. *Intra*molecular electron transfer occurs in the inner-sphere bridged precursor to give A–B and this is followed by a dissociation of the A–B complex to give the products.

$$A + B \underset{k_{-1}}{\overset{k_1}{\rightleftharpoons}} (A\text{–}B)$$

$$(A\text{–}B)^* \underset{k_{-2}}{\overset{k_2}{\rightleftharpoons}} A\text{–}B$$

$$A\text{–}B \xrightarrow{k_3} \text{products}$$

If the precursor (A–B)* has an appreciable lifetime, then the rate of *intra*molecular electron transfer in the precursor could be partially rate determining. Figure 11 shows a simplified plotting of a potential energy surface for the redox reaction of A and B to give products. There is a potential energy well on the left representing the electronic state of the separated ground-state reactants; the other potential energy well on the right represents the electronic state of the separated products. Where the two energy wells (or surfaces) intersect there is a set of nuclear configurations for which $E_R = E_P$. The two electronic states interact in this region with the energy of the interaction called a "resonance" energy, ΔE. If this resonance energy or gap is sufficiently large, i.e., greater than ca. 0.5 kcal (=175 cm^{-1}), then the electron transfer is adiabatic and the system will remain on the lower curve as it traverses the energy barrier. In the case of an adiabatic electron transfer, the orbital overlap in the precursor is favorable and the *intra*molecular electron transfer is fast compared to the lifetime of the precursor.

The more intriguing situation is where the resonance energy is small and nonadiabatic electron transfer occurs between A and B. In reference to Figure 11, this is the case when ΔE is small. In a nonadiabatic electron transfer the system does not always stay on the lower surface, but it will "jump" to the higher energy surface. The probability of crossing from the reactants to the products is reduced. The lifetime of the precursor is short relative to the rate of *intra*molecular electron transfer in the precursor. In such a nonadiabatic electron transfer the rate will depend on the resonance energy of interaction between the potential wells for the reactants and products. In a recent paper, Taube[62] has summarized the experimental evidence for nonadiabaticity in solution oxidation–reduction reactions to show that it is difficult to determine if a given reaction is nonadiabatic. A few examples of possible nonadiabatic reactions were mentioned.

It seems quite reasonable that, if the redox reaction between transition–metal complexes A and B is assumed to be of the inner-sphere type and in the precursor there is a very extended bridging molecular unit interposed between the two transition-metal centers, the resonance energy could be small and this would lead to nonadiabatic electron transfer. The precursor forms with the extended inner-sphere bridge and it takes a relatively long time for the electron transfer. It is the electronic structure, i.e., orbital compositions and energies, of the extended bridging unit as it interfaces with the characteristics of the two metal complexes that determine the magnitude of the resonance energy. Qualitatively, then, it can be understood why the characterization of the viability of a given bridge to support an antiferromagnetic interaction can be useful to understand whether that same bridging unit would tend to lead to nonadiabatic electron transfer. The occurrence of appreciable magnetic exchange interaction in a binuclear complex means that the electronic state manifolds of the two metal complexes have coupled effectively to produce a delocalized electronic structure for the binuclear complex. Thus, if a particular extended bridge is indicated as the electron transfer pathway in an inner-sphere redox reaction, in theory the viability of the bridge to provide coupling between two electronic manifolds can be gauged by preparing a stable binuclear complex with two paramagnetic metal ions having ground-state electron configurations and electronic states similar to those in the two redox-active metal complexes.

Oxidation–reduction reactions between Cr^{2+} (or V^{2+}) and $Co(NH_3)_5(^-O_2C(bph)CO_2^-)^+$ (bph = 4,4′-biphenylyl) have suggested that the electron transfer occurs through the bridging organic acid group.[63] The electron transferred in the precursor comes from a π-type t_{2g} orbital for V^{2+} (σ-type e_g orbital for Cr^{2+}) and transfers into a σ-type e_g orbital. In our work with the $[Cu_2(tren)_2(BZD)](Y)_4$ complexes we found that two σ-type electronic manifolds (d_{z^2} ground states) could be coupled by the benzidine unit. The antiferromagnetic interaction was quite weak, however. The molecular orbital calculations for benzidine showed that the degree of σ and π mixing could be sensitive to the dihedral angle between the two phenyl rings in the bridge.

Conclusions

The first stable nonpolymeric complexes between aromatic diamines such as BZD or PPD and copper(II) have been prepared and characterized using variable-temperature magnetic susceptibility and EPR. The discrete nature of the binuclear complexes was revealed in the X-ray diffraction study of $[Cu_2(tren)_2(BZD)](NO_3)_4$. All copper(II) complexes bridged by aromatic diamines show antiferromagnetic exchange interactions with exchange parameters which range from ca. -3 cm^{-1} for the BZD-bridged complexes to nearly -35 cm^{-1} for the complexes bridged by PPD. A molecular orbital analysis reveals that the superexchange mechanism predominantly involves the σ orbitals of the aromatic diamines but π orbitals may also be used in a spin-polarization pathway. The structurally characterized $[Cu_2(tren)_2(BZD)](NO_3)_4$ complex shows that electrons may exchange between two

copper(II) centers separated by more than 12 Å including a C–C single bond in the exchange pathway. The d_{z^2} orbital seems particularly effective in propagating exchange interactions across an extended bridging group. Binuclear complexes formed between $VO(hfac)_2$ and PPD or DDA do not exhibit any exchange coupling, but the BZD-bridged complex gave the anomalous result of one-unpaired electron per binuclear complex. Finally, the interrelationships between a superexchange interaction and an inner-sphere electron-transfer process were presented.

Acknowledgment. We are grateful for the partial support of this research from National Institutes of Health Grant HL 13652 and for computing funds provided by the University of Illinois Research Board.

Appendix

The spin Hamiltonian in eq 2 assumes that the g values for each Cu(II) ion are equal. Additionally, the spin operators $-J\hat{S}_1^2$ and $-J\hat{S}_2^2$ have been dropped since these contribute a constant amount to each energy level. The four singlet–triplet wave functions can be expressed in the coupled basis set, $|S\ M_s\rangle$, as follows:

$$|0\ 0\rangle = \frac{1}{\sqrt{2}}\left|\tfrac{1}{2}\ -\tfrac{1}{2}\right\rangle - \frac{1}{\sqrt{2}}\left|-\tfrac{1}{2}\ \tfrac{1}{2}\right\rangle$$

$$|1\ -1\rangle = \left|-\tfrac{1}{2}\ -\tfrac{1}{2}\right\rangle$$

$$|1\ 0\rangle = \frac{1}{\sqrt{2}}\left|\tfrac{1}{2}\ -\tfrac{1}{2}\right\rangle + \frac{1}{\sqrt{2}}\left|-\tfrac{1}{2}\ \tfrac{1}{2}\right\rangle$$

$$|1\ 1\rangle = \left|\tfrac{1}{2}\ \tfrac{1}{2}\right\rangle$$

The kets on the right side of the above four equations represent the uncoupled basis functions (given by $|M_{s_1}\ M_{s_2}\rangle$ such that $S = S_1 + S_2$ and $M_s = M_{s_1} + M_{s_2}$) preceded by the appropriate Clebsch–Gordon coefficient. When the Hamiltonian operator $\hat{H}$ in eq 2 operates on the coupled basis set for two spin = $^1/_2$ centers ($S_1 = S_2 = {}^1/_2$), the nonzero matrix elements in the upper right triangle of the 4 × 4 energy matrix are

$$\langle 1\ -1|\hat{H}|1\ -1\rangle = -2J - g_\parallel \beta H$$

$$\langle 1\ 0|\hat{H}|1\ 0\rangle = -2J$$

$$\langle 1\ 1|\hat{H}|1\ 1\rangle = -2J + g_\parallel \beta H$$

$$\langle 1\ -1|\hat{H}|1\ 0\rangle = \langle 1\ 0|\hat{H}|1\ 1\rangle = \frac{\sqrt{2}}{2} g_\perp \beta H$$

The $g_\parallel$ and $g_\perp$ values for each compound were obtained from the 300 K Q-band EPR spectrum. The magnetic susceptibilities were measured with a field strength of $H = 12.7$ kG and, hence, the magnetic moment may be evaluated as

$$\mu_i = -\partial E_i / \partial H$$

where E_i is the energy of the ith state. The difference in energy levels as a function of the magnetic field may be used to obtain the magnetic moments. The parallel and perpendicular molar susceptibilities may then be calculated from

$$\chi_\alpha = \frac{N}{H} \frac{\sum_i (-\partial E_i/\partial H)\ \exp(-E_i/kT)}{\sum_i \exp(-E_i/kT)}$$

where $\alpha = x$, y, or z and N is Avogadro's number. The energy matrix was diagonalized to give $\chi_\parallel$ and $\chi_\perp$. The total molar susceptibility was taken as

$$\chi_M = {}^1/_3\chi_\parallel + {}^2/_3\chi_\perp + N\alpha$$

where $N\alpha$ is the temperature-independent paramagnetism.

The diagonalizations were combined with a least-squares minimization procedure to obtain the best fit with the three variable parameters J, $g_\parallel$, and $g_\perp$.

Registry No. $[Cu_2(tren)_2(BZD)](NO_3)_4$, 65776-91-2; $[Cu_2(tren)_2(BZD)](ClO_4)_4$, 65830-13-9; $[Cu_2(tren)_2(BZD)](PF_6)_4$, 65941-80-2; $[Cu_2(tren)_2(OT)](PF_6)_4$, 65776-93-4; $[Cu_2(tren)_2(MDA)](NO_3)_4$, 67180-37-4; $[Cu_2(tren)_2(MDA)](ClO_4)_4$, 67225-87-0; $[Cu_2(tren)_2(PPD)](NO_3)_4$, 65776-95-6; $[Cu_2(tren)_2(PPD)](ClO_4)_4$, 67314-00-5; $[Cu_2(tren)_2(PPD)](PF_6)_4$, 67314-01-6; $[Cu_2(tren)_2(DDA)](PF_6)_4$, 67180-39-6; $[VO(hfac)_2]_2(BZD)$, 67180-40-9; $[VO(hfac)_2]_2(PPD)$, 67180-41-0; $[VO(hfac)_2]_2(DDA)$, 67180-42-1; $VO(hfac)_2$, 15819-88-2.

Supplementary Material Available: Tables I (analytical data), II–V (experimental and calculated magnetic susceptibility data for four binuclear Cu(II) complexes bridged by benzidine or *o*-tolidine), VI (experimental magnetic susceptibility data for two binuclear Cu(II) complexes bridged by MDA), VII–X (experimental and calculated magnetic susceptibility data for four binuclear Cu(II) complexes bridged by *p*-phenylenediamine or durenediamine), and XI (experimental magnetic susceptibility data for three $VO(hfac)_2$ binuclear complexes bridged by *p*-phenylenediamine, durenediamine, or benzidine) (20 pages). Ordering information is given on any current masthead page.

References and Notes

(1) Part 16: S. L. Kessel and D. N. Hendrickson, *Inorg. Chem.*, **17**, 2630 (1978).
(2) Camille and Henry Dreyfus Fellow, 1972–1977; A. P. Sloan Foundation Fellow, 1976–1978.
(3) Part 1: D. M. Duggan, E. K. Barefield, and D. N. Hendrickson, *Inorg. Chem.*, **12**, 985 (1973).
(4) Part 2: D. M. Duggan and D. N. Hendrickson, *Inorg. Chem.*, **12**, 2422 (1973).
(5) Part 3: D. M. Duggan and D. N. Hendrickson, *Inorg. Chem.*, **13**, 2929 (1974).
(6) Part 4: D. M. Duggan and D. N. Hendrickson, *Inorg. Chem.*, **14**, 1944 (1975).
(7) Part 5: G. R. Hall, D. M. Duggan, and D. N. Hendrickson, *Inorg. Chem.*, **14**, 1956 (1975).
(8) Part 6: K. R. Mann, D. M. Duggan, and D. N. Hendrickson, *Inorg. Chem.*, **14**, 2577 (1975).
(9) Part 7: E. J. Laskowski, D. M. Duggan, and D. N. Hendrickson, *Inorg. Chem.*, **14**, 2449 (1975).
(10) Part 8: E. J. Laskowski, T. R. Felthouse, D. N. Hendrickson, and G. J. Long, *Inorg. Chem.*, **15**, 2908 (1976).
(11) Part 9: D. S. Bieksza and D. N. Hendrickson, *Inorg. Chem.*, **16**, 924 (1977).
(12) Part 10: T. R. Felthouse, E. J. Laskowski, and D. N. Hendrickson, *Inorg. Chem.*, **16**, 1077 (1977).
(13) Part 11: C. G. Pierpont, L. C. Francesconi, and D. N. Hendrickson, *Inorg. Chem.*, **16**, 2367 (1977).
(14) Part 12: T. R. Felthouse and D. N. Hendrickson, *Inorg. Chem.*, **17**, 444 (1978).
(15) Part 13: E. J. Laskowski and D. N. Hendrickson, *Inorg. Chem.*, **17**, 457 (1978).
(16) Part 14: E. F. Hasty, L. J. Wilson, and D. N. Hendrickson, *Inorg. Chem.*, **17**, 1834 (1978).
(17) D. M. Duggan, R. G. Jungst, K. R. Mann, G. D. Stucky, and D. N. Hendrickson, *J. Am. Chem. Soc.*, **96**, 3443 (1974).
(18) Part 15: M. S. Haddad and D. N. Hendrickson, *Inorg. Chem.*, **17**, 2622 (1978).
(19) D. M. Duggan and D. N. Hendrickson, *Inorg. Chem.*, **13**, 1911 (1974).
(20) H. W. Richardson and W. E. Hatfield, *J. Am. Chem. Soc.*, **98**, 835 (1976), and references therein; M. Koyama, H. Suzuki, and T. Watanabe, *J. Phys. Soc. Jpn.*, **40**, 1564 (1976).
(21) H. W. Richardson, J. R. Wasson, and W. E. Hatfield, *Inorg. Chem.*, **16**, 484 (1977).
(22) M. S. Haddad, D. N. Hendrickson, J. P. Cannady, R. S. Drago, and D. S. Bieksza, to be submitted for publication.
(23) R. W. Callahan, G. M. Brown, and T. J. Meyer, *Inorg. Chem.*, **14**, 1443 (1975), and references therein.
(24) R. W. Callahan, F. R. Keene, T. J. Meyer, and D. J. Salmon, *J. Am. Chem. Soc.*, **99**, 1064 (1977).
(25) B. C. Bunker, R. S. Drago, D. N. Hendrickson, R. M. Richman, and S. L. Kessel, *J. Am. Chem. Soc.*, **100**, 3805 (1978).
(26) H. Fischer, G. M. Tom, and H. Taube, *J. Am. Chem. Soc.*, **98**, 5512 (1976), and references therein.
(27) J. M. Malin, D. A. Ryan, and T. V. O'Halloran, *J. Am. Chem. Soc.*, **100**, 2097 (1978).
(28) T. R. Felthouse, E. N. Duesler, and D. N. Hendrickson, *J. Am. Chem. Soc.*, **100**, 618 (1978).
(29) Supplementary material.
(30) The further reaction of PPD to yield a brown solid is under investigation. In the case of $[Cu_2(tren)_2(PPD)](PF_6)_4$, a microcrystalline brown solid

formed upon repeated recrystallization from methanol or acetone which differed in elemental composition from the green product. The brown product forms in both the presence and absence of oxygen from a solution of the green product.
(31) R. L. Carlin and F. A. Walker, Jr., *J. Am. Chem. Soc.*, **87**, 2128 (1965).
(32) B. N. Figgis and J. Lewis, in "Modern Coordination Chemistry", J. Lewis and R. G. Wilkins, Ed., Interscience, New York, N.Y., 1960, p 403.
(33) J. P. Chandler, Program 66, Quantum Chemistry Program Exchange, Indiana University, Bloomington, Ind., 1973.
(34) J. A. Pople and D. L. Beveridge, "Approximate Molecular Orbital Theory", McGraw-Hill, New York, N.Y., 1970.
(35) B. Bleaney and K. D. Bowers, *Proc. R. Soc. London, Ser. A*, **214**, 451 (1952).
(36) B. J. Hathaway and D. E. Billing, *Coord. Chem. Rev.*, **5**, 143 (1970).
(37) P. C. Jain and E. C. Lingafelter, *J. Am. Chem. Soc.*, **89**, 6131 (1967).
(38) J. A. Fee, *Struct. Bonding (Berlin)*, **23**, 1 (1975), and references therein; E. Frieden and H. S. Hsieh, *Adv. Enzymol. Relat. Areas Mol. Biol.*, **44**, 187 (1976), and references therein.
(39) B. E. Myers, L. Berger, and S. A. Friedberg, *J. Appl. Phys.*, **40**, 1149 (1969).
(40) M. W. Van Tol, K. M. Diederix, and N. J. Poulis, *Physica (Utrecht)*, **64**, 363 (1973).
(41) S. N. Bhatia, C. J. O'Connor, R. L. Carlin, H. A. Algra, and L. J. DeJongh, *Chem. Phys. Lett.*, **50**, 353 (1977).
(42) B. Morosin, *Acta Crystallogr., Sect. B*, **26**, 1203 (1970).
(43) B. Morosin, *Acta Crystallogr., Sect. B*, **32**, 1237 (1976).
(44) F. A. Walker, R. L. Carlin, and P. H. Rieger, *J. Chem. Phys.*, **45**, 4181 (1966).
(45) B. A. Goodman and J. B. Raynor, *Adv. Inorg. Chem. Radiochem.*, **13**, 235 (1970).
(46) B. C. Saunders, in "Inorganic Biochemistry", Vol. 2, G. L. Eichhorn, Elsevier, 1973, Chapter 28, and references therein.
(47) For example, see C. Heitner-Wirguin and J. Selbin, *J. Inorg. Nucl. Chem.*, **30**, 3181 (1968).
(48) P. J. Hay, J. C. Thibeault, and R. Hoffmann, *J. Am. Chem. Soc.*, **97**, 4884 (1975).
(49) E. F. Hasty, T. J. Colburn, and D. N. Hendrickson, *Inorg. Chem.*, **12**, 2414 (1973).
(50) A. P. Ginsberg, *Inorg. Chim. Acta, Rev.*, **5**, 45 (1971).
(51) W. Heisenberg, *Z. Phys.*, **49**, 619 (1928).
(52) P. A. M. Dirac, *Proc. R. Soc. London, Ser. A*, **123**, 714 (1929).
(53) P. A. M. Dirac, "The Principles of Quantum Mechanics", 3rd ed, Oxford University Press, London, 1947, Chapter 9.
(54) D. Kivelson, *J. Chem. Phys.*, **33**, 1094 (1960).
(55) J. D. Currin, *Phys. Rev.*, **126**, 1995 (1962).
(56) J. H. Freed, *J. Chem. Phys.*, **45**, 3452 (1966).
(57) C. S. Johnson, *Mol. Phys.*, **12**, 25 (1967).
(58) M. P. Eastman, R. G. Kooser, M. R. Das, and J. H. Freed, *J. Chem. Phys.*, **51**, 2690 (1969); J. H. Freed, *J. Phys. Chem.*, **71**, 38 (1967); M. P. Eastman, G. V. Bruno and J. H. Freed, *J. Chem. Phys.*, **52**, 321 (1970).
(59) W. L. Reynolds and R. M. Lumry, "Mechanisms of Electron Transfer", Ronald Press, New York, N.Y., 1966.
(60) R. A. Marcus, *Annu. Rev. Phys. Chem.*, **15**, 155 (1964).
(61) J. Halpern, *Q. Rev., Chem. Soc.*, **15**, 207 (1961).
(62) H. Taube, *Adv. Chem. Ser.*, **No. 162**, 127–144 (1977).
(63) R. T. M. Fraser, *J. Am. Chem. Soc.*, **83**, 4920 (1961).

Contribution from the Department of Chemistry, Cornell University, Ithaca, New York 14853

Relative Strengths of Axial and Equatorial Bonds and Site Preferences for Ligand Substitution in σ-Bonded Trigonal- and Pentagonal-Bipyramidal Complexes

EVGENY SHUSTOROVICH[1]

Received February 14, 1978

For bipyramidal trigonal (TB) EL_5 D_{3h} and pentagonal (PB) EL_7 D_{5h} complexes (E is a transition metal M or main-group element A) two problems have been considered: (1) the relative strengths of axial (ax) and equatorial (eq) bonds and (2) the site preferences (SP) of stronger donor (or acceptor) substituents L′. An analytical approach has been developed in the framework of canonical LCAO MO theory. Ratios of overlap populations $T = N_{eq}/N_{ax}$ were estimated for *n*s, *n*p, and $(n-1)$d contributions producing values of $1 < T^{(s)}$, $1 < T^{(p)} < 1.15$, $T^{(d^0-d^4)} \approx 1.5$, and $T^{(d^8)} \approx 0.3$ for TB complexes and $T^{(s)} < 1$, $0.9 < T^{(p)} < 1$, and $T^{(d^0-d^4)} \approx 1.2$ for PB complexes. The contributions all reinforce to make equatorial bonds relatively stronger than axial bonds, eq > ax, in AL_5 and ML_5 (d^0–d^4) complexes while the $T^{(d^8)}$ contribution dominates in ML_5 (d^8) complexes to make ax ≥ eq. The perturbing influence of $(n-1)d^{10}$ shells in AL_5 complexes was also examined and found capable of making ax > eq under certain conditions. The opposing contributions of s, p, and d in ML_7 (d^0–d^4) complexes equalize axial and equatorial bonds while s and p contributions predominate in AL_7 complexes resulting in ax > eq. SP for substituents were examined using perturbation theory with the finding that a stronger donor ligand will substitute equatorially in AL_5 and ML_5 (d^0–d^4) complexes and axially in ML_5 (d^8) and AL_7 complexes. Quantitative details must be considered in ML_5 (d^{10}) and ML_7 (d^0–d^4) cases. The relationship between bond energy and bond polarity criteria for SP (equivalent in some instances) was examined for all cases. The results obtained agree with the available experimental and computational data and permit a number of predictions to be made.

Introduction

By tradition most studies on the electronic and geometric structures of coordination compounds are devoted to the square or tetrahedral EL_4 and octahedral EL_6 complexes (E is a transition metal M or a main-group element atom A). In these polyhedra with very high symmetry all the ligands are geometrically equivalent, permitting symmetry arguments to be used most effectively. That, in turn, makes reliable many results obtained from a variety of approximate models. In particular, the theory of the mutual influence of ligands (MIL) has been developed only for square and octahedral complexes where all valence angles are equal to 90 or 180° reducing the MIL to the trans–cis influence.[2-5]

In recent years one can observe the sharply increasing interest in EL_5 and EL_7 polyhedra where all ligand positions can not be equivalent. Most effort has been directed to the problem of the relative stability of different possible polyhedra for a given composition EL_m and the barriers to their interconversion.[6-18] The present work will not address this problem but consider only bipyramidal structures, trigonal (TB) EL_5 and pentagonal (PB) EL_7. The difference between axial, $E-L_{ax}$, and equatorial, $E-L_{eq}$, bonds generates three specific problems of structure for these compounds (as compared with square and octahedral ones): (1) the relative strengths of the $E-L_{ax}$ and $E-L_{eq}$ bonds in unsubstituted complexes EL_m; (2) the site preference of a given substituent L′ for an axial or equatorial position under substitution $EL_m \rightarrow EL_{m-1}L'$; (3) differences in the influence of the ligand L′, in a substituted $EL_{m-1}L'$ complex, on the strength of the initial axial and equatorial bonds.

Sufficient experimental data exist for a discussion of some fundamental regularities in the structure of these complexes, especially EL_5. Moreover, quantitative quantum chemical calculations have been performed on specific EL_5[8,9,15-18] and

0020-1669/78/1317-2648$01.00/0